Single-Mode Multicore Fibers With Integrated Bragg Filters

Martin Becker, Adrian Lorenz, Tino Elsmann, Ines Latka, Anka Schwuchow, Sebastian Dochow, Ron Spittel, Jens Kobelke, Jörg Bierlich, Kay Schuster, Manfred Rothhardt, and Hartmut Bartelt

Abstract—Fiber Bragg gratings (FBGs) in single-mode fibers, used as narrowband filters, have reached a high maturity level, especially for applications in telecommunications and sensing. In spectroscopic applications, e.g., in Raman spectroscopy, FBG filters can be used to separate laser probing light from generated sensor light which simplifies Raman probes. For this purpose, light from a sample has to be collected with high efficiency into a fiber. The light collection efficiency in single-mode fibers is, however, strongly limited due to the small fiber core area. Therefore, we have investigated the possibility to use single-mode multicore fibers to increase the light collection efficiency while maintaining Bragg filter performance. An optical density filtering effect of 1.5, which is equivalent to a transmission of −15 dB, has been achieved with a FBG in a 61-core fiber. Simulations have been performed in order to clarify the influence of the fiber geometry and refractive index distribution on grating performance. The application of chirped gratings in the multicore fibers improves filter performance in comparison to homogeneous gratings.

Index Terms—Bragg filter, microstructured optical fiber, optical fiber filters, two-beam interferometry.

I. INTRODUCTION

SPECTRAL filtering in compact fiber devices is an important key element in spectroscopical applications, e.g., for astronomy and the life sciences. Typical applications include the suppression of atmospheric fingerprints coming from the sky in the infrared wavelength region [1]. With respect to the life sciences, Raman spectroscopy is used to discriminate, e.g., between normal and pathological tissue which helps to reduce resections. Here, the suppression of the excitation laser wavelength is a comparable problem. One mandatory filter is a notch filter in the detection path suppressing elastically scattered laser light. Actual fiber-coupled Raman probes for field detection are reported to be excellent for biosensing [2], but in-vivo applications inside the human body require miniaturization of the sensing probes. For this purpose and for fail safe assembly, an all fiber solution with no external optical parts is desirable. Fiber

Bragg gratings (FBGs) are very well suited for this task as they are in-line and can be made with high blocking ratio. As demonstrated many times, thin film filters are also appropriate for this filtering purpose, but require a complex assembly [3], [4].

In Raman spectroscopy, only a small fraction of the incident light is Raman scattered. As laser-induced heating of the sample limits the amount of light that can be delivered to the sample, maximal light collection is crucial for a good performance of the probes [5].

Efficient Bragg filter devices in single mode fibers, which have reached a high level of maturity in optical telecommunication [6], cannot be applied directly for such demands.

Multi-core fibers (MCFs) with tapers as interface to multimode ports ("photonic lantern") have been proposed to maintain Bragg filtering properties of the fiber and to provide efficient light collection [7]–[11]. In order to avoid taper interfaces we have investigated the filtering effect of FBGs directly in multicore single-mode fibers (SM-MCFs). This fiber type has been designed to combine good light collection properties with efficient Bragg filtering, while maintaining the advantages of an integrated optical fiber solution. For this approach it is of great importance that all individual core gratings (ICGs) of the MCF are reflecting at the same wavelength and show a strong filtering effect [7], [10]. We discuss the light collecting efficiency of single and multicore optical fibers, analyze the filtering efficiency and consider the influence of the multicore structure on the FBG inscription.

II. THEORY OF LIGHT COLLECTION AND FILTERING EFFICIENCY

The light collection efficiency of an optical fiber that captures light from a Lambertian surface is defined by the étendue Θ [3]:

$$\Theta = \left(\frac{1}{2}\pi d_{\text{core}} N A\right)^2, \tag{1}$$

where d_{core} is the core diameter and NA is the numerical aperture. The amount of light that can be coupled into the optical fiber may be increased by a larger acceptance angle $\sin \alpha = NA$ of the fiber or by a larger diameter of the fiber core.

Eq. (1) indicates a relationship of the étendue and the fiber parameter V:

$$V = \frac{\pi d_{\text{core}}}{\lambda} N A. \tag{2}$$

λ is the vacuum wavelength. The number of guided modes M in a (step index) fiber [12] is approximately proportional to the
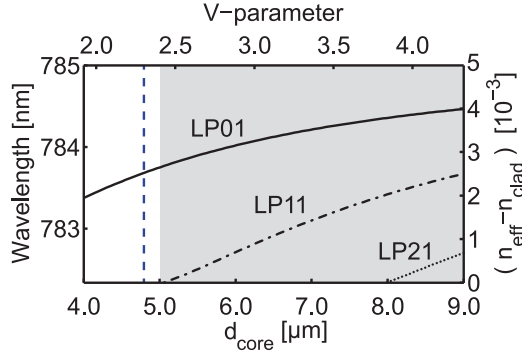
Fig. 1. Calculated FBG reflection wavelength for a step index waveguide with $NA = 0.12$. The shaded area indicates multi-mode operation. The vertical dashed line indicates the cutoff criterion described in Section III.

Fig. 2. Wavelength splitting of supermode bandstructure (top- and bottom-band edge) in a periodic hexagonal arrangement for different distances Λ. The unshaded area indicates the acceptable spectral bandwidth of the filter and the vertical line marks the minimal tolerable distance of two cores.

étendue:

$$M \approx \frac{V^2}{2} = 2\frac{\Theta}{\lambda^2}. \tag{3}$$

This equation reveals a direct relation between the amount of light that is captured by the waveguide and the number of guided modes. The rise of higher order modes affects FBG filtering efficiency. Different modes in a waveguide lead to wavelength spreading of the Bragg reflections [13]–[15]:

$$\lambda_{\text{Bragg}}(i, j) = (n_i + n_j) \Lambda_{\text{Bragg}} \tag{4}$$

where n_i and n_j are the effective refractive indices for the modes i and j. Λ_{Bragg} is the grating period inside of the fiber and λ_{Bragg} is the resulting Bragg reflection wavelength. Each mode ($i = j$) leads to an individual Bragg reflection wavelength, and coupling between different modes ($i \neq j$) results in additional reflection peaks. When efficient Bragg filtering is required, all these modes must reflect within the Bragg reflection bandwidth. For a strong FBG with homogeneous (unchirped) index-modulation distribution, one can estimate the notch filter bandwidth as [16]:

$$2\Delta\lambda_{\text{Bragg}} \approx \frac{\lambda_{\text{Bragg}}^2}{\pi n_{\text{eff}}L}\text{arctanh}\sqrt{R}. \tag{5}$$

Fig. 1 shows the calculated FBG reflection wavelengths for different modes in a step index fiber for a fixed Bragg period $\Lambda_{\text{Bragg}} = 270$ nm. The V-parameter of the fiber is tuned by variation of the core diameter between 4 and 9 μm. The step index of the core remains constant ($\Delta n_{\text{core}} = 5 \times 10^{-3}$). The calculation indicates that the wavelength spacing between different reflection peaks is in the range of 1 to 2 nm. In case of a typical homogeneous grating (5 mm grating length, 785 nm reflection wavelength) and an optical density of OD4 ($R = 99.99\%$), Eq. (5) yields a FWHM of 0.14 nm. Such a grating can efficiently reflect only in a single mode fiber. Therefore, in this case only fibers with a V-parameter below 2.405 can be used. At higher values it is possible that a portion of the transmitted light propagates through higher order modes, for which the Bragg reflection wavelength is shifted to lower values and passes the FBG at the Bragg reflection wavelength of the fundamental mode [17]. For a more efficient filtering of several modes, the filter bandwidth should exceed the
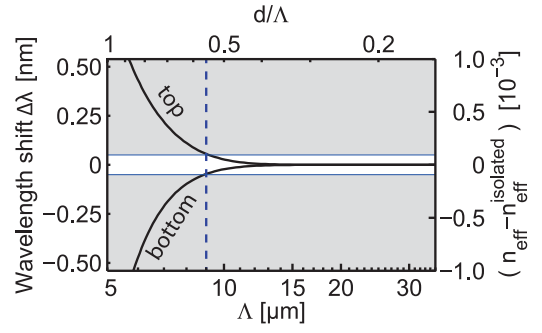
wavelength distance of the different modes, e.g., by using a chirped grating.

III. OPTICAL MCF DESIGN

In the present case we have designed and drawn a multi-core single-mode fiber according to the principles established in reference [18] which include the maximization of the étendue per unit cell. In order to increase the light collection efficiency while maintaining a good filtering, our fiber design comprises a close hexagonal packing of multiple single-mode cores. In this case, the effective étendue per unit cell area A_{UC} can be described by:

$$\frac{\Theta}{A_{\text{UC}}} = \frac{\left(\frac{1}{2}\pi d_{\text{core}}NA\right)^2}{\frac{\sqrt{3}}{2}\Lambda^2}. \tag{6}$$

According to Eq. (6), the center-to-center distance of the cores Λ should be made as small as possible. However, a decrease of Λ will result in an enhanced coupling between the cores, leading to the formation of supermodes and a band-structure of the effective refractive indices (see Fig. 2). In the case of a given Bragg grating bandwidth, the allowed distance of the cores has a lower limit. The limit is given by the maximum spectral filter width to ensure an effective filtering for all modes at the operation wavelength. According to Eq. (5), the reflection bandwidth of an unchirped FBG is 0.14 nm; therefore, the maximum allowed splitting was chosen to be 0.1 nm. Due to given preform parameters (see Section IV), the numerical aperture has a value of $NA = 0.12$. The cutoff of the single (isolated) core was chosen to be 735 nm in order to ensure single-mode operation at the operation wavelength (785 nm) even in the presence of variations due to manufacturing tolerances. This results in a core diameter of $d_{\text{core}} = 4.7$ μm and V-parameter of ≈ 2.3 at $\lambda = 785$ nm (see Fig. 1). As reported in previous publications, core-to-core coupling affects the effective index of the individual cores. This leads to a splitting of the effective refractive indexes due to MCF supermodes. This splitting has to be kept below a certain limit in order to prevent broadening of the ICG spectra [7], [10], [18]. To optimize the core spacing Λ, we set up an infinite lattice of corresponding single-mode cores and
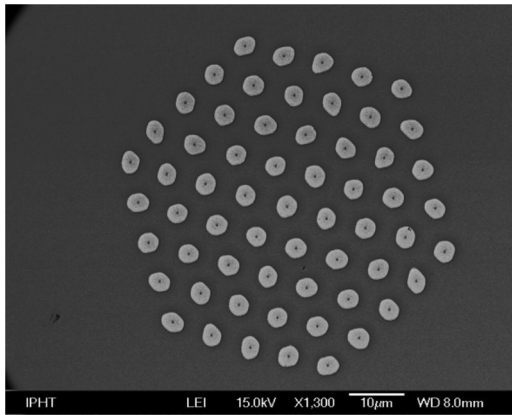
Fig. 3. REM image of the 61-core single-mode MCF. The fiber end-face was etched to increase contrast.
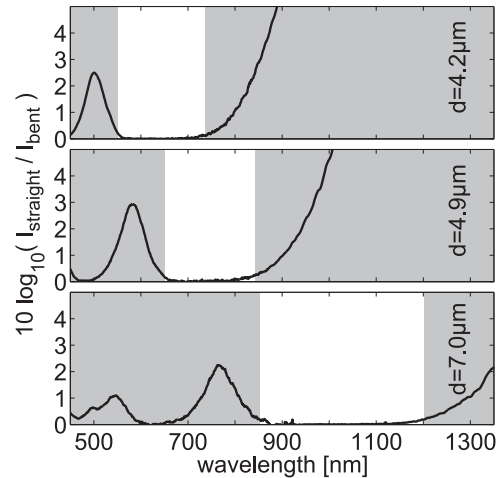

Fig. 4. Cutoff measurement of the 61-core fiber with core diameters between 4.2 and 7.0 μm. The filling factor is $d/\Lambda = 0.54$. The white area indicates the operational window for the different fibers. The single-bend attenuation method has been applied.
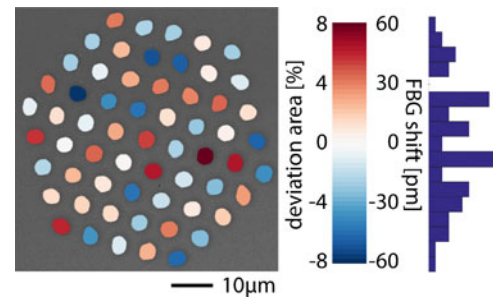

Fig. 5. Expected Bragg wavelength variations due to different core sizes and corresponding histogram of core size distribution (right). The color bar axis scalings are equivalent and show the relative deviation of the core area from the mean value as well as corresponding shift of FBG central wavelength. The color bar belongs to the colored REM image and the histogram.

calculated the top- and bottom-band edge of the resulting band structure of the LP01 modes using a semi-analytical model [19]. The difference of the effective refractive indices of both band edges is then used to calculate the maximum spectral splitting of the FBG resonances. Calculation results are shown in Fig. 2, which indicates an optimized pitch of $\Lambda = 9$ μm.

IV. EXPERIMENTAL OPTICAL FIBER

Following the fiber design, a 61-core fiber was manufactured using the stack-and-draw technology. The primary preform for fabricating the doped cores was prepared by the MCVD method. The core clad ratio d/Λ was adjusted by etching the primary preform with hydrofluoric acid before stretching into core packaging rods. They were arranged in a four-ring hexagonal package. To minimize deformations of the outer rings, the interspace between hexagonal arrangement and overcladding tube was filled with geometrically adapted undoped silica rods (Heraeus Suprasil F300). To obtain a compact solid fiber, the fiber was drawn while evacuating the interspace volume of the package [20]. The fiber cores have a dopant concentration of 6 mol-% GeO_2 and 7 mol-% B_2O_3, which gives a theoretical numerical aperture of $NA = 0.12$. Fibers with different core sizes but with the same filling factor from the same preform were drawn with parameters close to the design parameters. The cutoff wavelength was measured by the differential single-bend attenuation method [21] with a mandrel diameter of 30 mm. For the performed measurements we used a tungsten light source coupled to the fiber using full excitation and recording transmission directly with a spectrometer (Instrument Systems). The cutoff wavelength is defined as the point where the difference in transmission between bend and straight fiber is 0.1 dB (on the long-wavelength side). The measurement results for fibers drawn from one preform but different core diameters are shown in Fig. 4. As observed in single-mode fibers [22], the cutoff wavelength increases with core diameter. The sample, whose operational wavelength fits in the operational window (white space in Fig. 4) between the cutoff (λ_c) and the rising influence of bend induced losses, was chosen as a target for FBG inscrip-

tion. The selected fiber has a core diameter of $d = 4.9$ μm, a pitch of $\Lambda = 9.1$ μm (see Fig. 3), and an experimental cutoff wavelength of 650 nm. In the selected fiber, different core sizes are observed, which can be attributed to the stacking of different canes [23]. As already discussed in reference [7], this has to be taken into account. Therefore, we measured a statistical variation of the core areas of approx. 15% using image-processing software ImageJ [24] from Fig. 3, which is comparable to mode field area tolerances in standard single-mode fibers [25]. This leads to different effective Bragg reflection wavelengths at the same grating period. Assuming that there is no core-to-core variation of the NA, the resulting wavelength distribution was calculated from the different effective refractive mode indices, which are extracted from the simulation of the guided modes for the individual cores which are also retrieved from Fig. 3 and FEM-simulations. The results, shown in Fig. 5, indicate variations of the Bragg reflection wavelengths of about 120 pm. The core size and area spreading could be further improved, e.g., by the usage of hexagonal canes [23], [26]. However, the calculated maximum wavelength spreading is also considered to be
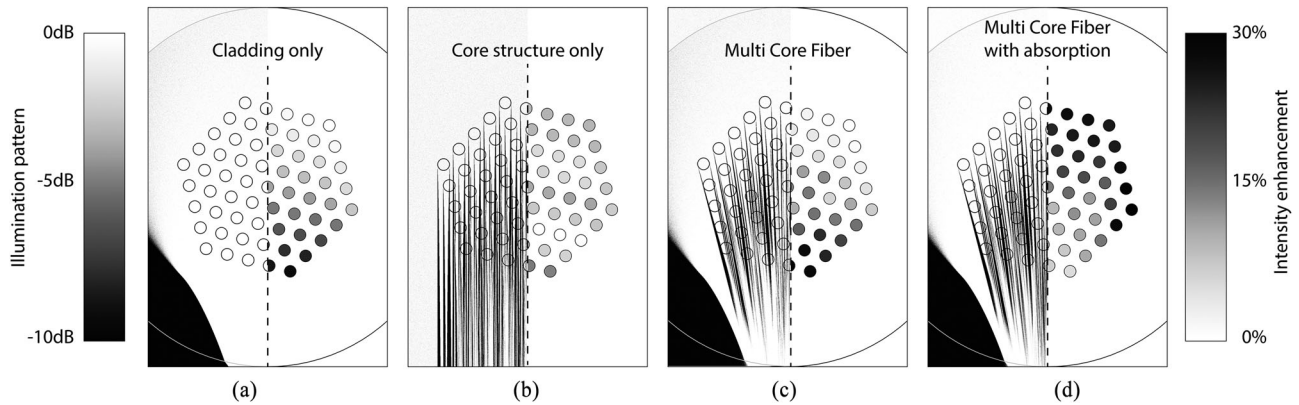
Fig. 6. Raytracing calculations of the light intensity distribution inside a 61-core SM-MCF regarding different effects, i.e., fiber lens function (a, c, and d), core lens function (b, c, and d), and light absorption of the cores (d). The fiber is illuminated from the top. The left side of each picture shows the illumination pattern with the intensity mapped on the left grayscale form average value (white 0 dB) to −10 dB below this value showing the inhomogeneous structure. The right side of each picture shows the averaged intensity within the cores. The grayscale shows the relative intensity enhancement based on the lowest single-core-intensity for each individual case.

suitable for an efficient Bragg-filter functionality. Additionally, due to the fiber fabrication process, a variation of the circularity of the cores is observed. The cores in the center tend to be more circular than the waveguides at the edges of the structure. Shape detection with the image processing software ImageJ reveals aspect ratios up to 1.38. According to reference [27], two effects resulting from the non-circularity influence the modal effective refractive index n_{eff}. First, there is an absolute shift due to a different overlap of the modal fields and the core area. Assuming same NA and same area for all cores this leads to Bragg-wavelength-shifts of up to 10 pm. The second effect is the birefringence within the cores arising from a main stress (5 pm) and a weak geometry related contribution (one order of magnitude lower). The stress-induced shift in the Bragg-wavelength is in the order of the absolute geometrically induced shift. Anyway, the wavelength-shift arising from different core sizes for the given fiber (60 pm) is one order of magnitude larger than the shift due to non-circularity. Therefore, influences of the non-circular shape of several cores are considered to be negligible for the filtering effect if the core area remains unchanged.

V. SIMULATION OF EXPOSURE CONDITIONS

To analyze the optical properties of the MCF during side illumination for FBG inscription, raytracing calculations (ZE-MAX) were done. Raytracing calculations are based on the assumption that interference between the surface layers of the micro-structure can be neglected. As discussed with a seven-core fiber used in [10], core-to-core shadowing during inscription should be taken into account. The considerable higher number of cores in our fiber makes it unavoidable. In our calculations, we have assumed an absorption coefficient of the doped core of 100 dB/mm for the inscription light at 248 nm. Absorption values from 27 dB/mm for a standard germanium doped fiber [28] up to 200 dB/mm at 240 nm for a photosensitive fiber [29] are reported in the literature. Compared to these values we considered that the pure silica cladding has no absorption. Calculation results are shown in Fig. 6. Four cases are shown,
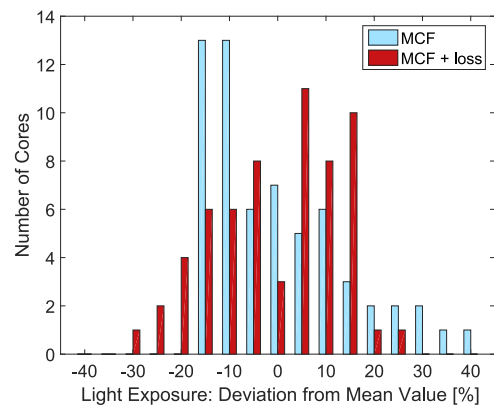

Fig. 7. Calculated statistical distribution of the light flux through the cores for a MCF without loss and for a MCF with UV-absorption (MCF + loss).

which cover the cylindrical lens function of the cladding, the cylindrical lens function of the cores, and the absorption. The results demonstrate that the light distribution inside the fiber is influenced by three main aspects: The fiber behaves as a cylindrical lens which forms a focal spot beyond the back side of the fiber [7], [8], [10]. The individual cores form a microlens array with focal lengths within the range of the multiple core array. Finally, absorption of UV-light in the cores results in a decay of the inscription intensity.

The lensing effect generates hot-spots at more distant cores, which causes the Bragg grating to increase faster during inscription at such positions, and the corresponding wavelength shift to become greater. Fig. 7 shows a distribution of the relative light flux through the cores under the assumption that the fiber acts as a cylindrical lens and the cores as a multiple lens array (cases c and d in Fig. 6). The graph shows two cases in parallel, i.e., without and with UV absorption in the cores. The nested lens array function of the SM-MCF leads to hot-spots towards the exit face. The absorption leads to cold spots in the same region, where grating growth is reduced. Such distributions now serve to calculate the SM-MCF FBG transmission function. To
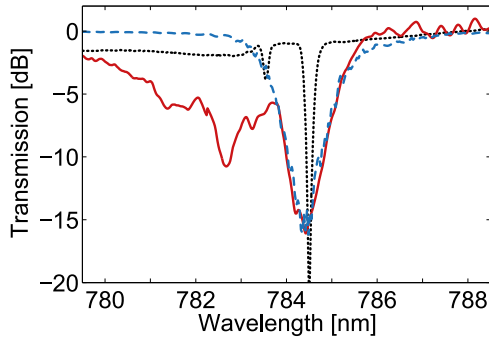
Fig. 8.   Measured transmission spectrum in a 61-core SM-MCF (solid red) in comparison to simulation (dashed blue) and single-core FBG in SMF (dotted black).

calculate transmission properties of the Bragg filter, the spreading of the effective refractive index of the individual cores due to the manufacturing conditions (see Fig. 5), and a distribution of the light flux through the cores during inscription (see Fig. 7) were taken into account. The flux distribution leads to distributions of the ICG reflection wavelength shift, strength, and spectral filter width during inscription. For homogeneous gratings, the transmission coefficients can be derived from the analytic solution of the coupled wave equations [30]. By combining the filtering effects of all different gratings in the array and assuming the same guided light intensity in all fiber cores, one can estimate the filtering characteristics of the complete core structure to be described as:

$$T(\lambda) = \frac{1}{N} \sum_{m=1}^{N} T_m(\lambda). \tag{7}$$

T_m are the transmission coefficients of the single cores m and N corresponds to the number of individual waveguides of the SM-MCF. This means in the case of an ideal grating in a 61-core SM-MCF, that one missing ICG limits the filter efficiency to -18 dB.

Due to the spreading of the core sizes, every core has its individual effective refractive index and therefore its own Bragg wavelength. During inscription, the wavelength shifts further because of the increase of the average refractive index due to a modulation index increase. The photoinduced refractive index change depends on the aforementioned illumination condition inside the fiber during grating inscription. Parameters selected for the calculation of the transmission profile of the FBG in a 61-core SM-MCF are $\Delta n_{\mathrm{mod}} = 2 \times 10^{-4}$ and a light distribution between 70% and 160% of the incoming light. Calculation results are shown in Fig. 8 for comparison with inscription experiments (Section VI).

VI. EXPERIMENTAL BRAGG FILTER INSCRIPTION

FBG inscription has been done with two beam interferometry and a KrF-excimer laser in MOPA configuration [31]. Hydrogen loading is applied [32] to increase the photosensitivity. In contrast to phase-mask inscription, where higher diffraction orders are involved [33], only the first diffraction orders of the holographic beam splitter are used for two-beam interferometry.

This prevents the interference of more than two beams, resulting in more homogeneous interference patterns across the fiber section [34]. Due to the combination of high-photon energy and high intensity of the applied laser system, index-matching fluids were not used in our experiments, to prevent high-intensity-related effects like out-gassing or carbonization [35] of the applied fluids. By coupling into a single core with single-mode fiber and light at 800 nm, we observed the near field pattern with a camera together with a cut-back method. We measured light spreading due to core-to-core coupling to be below 1 cm [36]. Above this fiber length, all cores appeared equally excited. Therefore, we considered the ICGs to act as an ensemble. The measured transmission spectrum in Fig. 8 shows a good overlap with the calculated spectrum at the operational wavelength region. The additional attenuation in the range of lower wavelengths is due to coupling into cladding modes, which is uncritical for the intended filtering application. The experimental result demonstrates that the discussed variations of the core structures can explain the characteristic transmission shape and the wavelength spreading of the SM-MCF FBG.

VII. WAVELENGTH SPREADING OF THE FBGS BY CORE VARIATIONS

It has been shown that the filtering efficiency of Bragg filter elements in SM-MCF is affected by mode and super-mode splitting (Eq. (4)), ICG spreading due to different core sizes (see Fig. 5), and different inscription conditions of the ICGs (see Fig. 7). All these effects cause wavelength mismatch of the ICGs. The limitation given by the filtering according to Eq. (5) was overcome by increasing the Bragg reflection bandwidth. One possible solution for this purpose is the increase in Bragg filter bandwidth obtained by raising the refractive index modulation. In practice, limitations arise due to the shift of the cutoff-wavelength during FBG inscription, the degradation of the grating due to saturation effects [37], and blurring of the grating structure due to instabilities of the experimental setup. Another promising solution is the application of chirped FBGs. As a feasibility study, we used a chirped phase-mask interferometer [31] for FBG-inscription in the SM-MCF. As a target fiber, we used a 19-core SM-MCF [18]. As shown in Fig. 6, the smaller amount of cores results in a higher optical density of the filter function which can be explained by reducing shadowing effects during inscription. The fiber was hydrogen loaded [32] to increase photosensitivity. Inscription time was 3 min, an increase of the filtering efficiency afterward was not observed. Results are shown in Fig. 9. For comparison, the figure also includes the experimental spectrum of an unchirped grating in the same fiber and the simulated transmission spectrum for the case of a chirped FBG ensemble. The chirped gratings are calculated via the step-chirped matrix approach [38] and the 19 core ICG spectra are merged with Eq. (7). The simulated curve assumes a refractive index increase of $\Delta n_{\mathrm{mod}} = 10^{-3}$, a chirp of 2.2 nm/cm, a grating length of 10 mm, and a spreading of the core exposure between 90% and 120% of the incoming light. The results in Fig. 9 indicate that chirped FBGs are a promising solution to cover a wider FBG wavelength spreading in MCFs. It
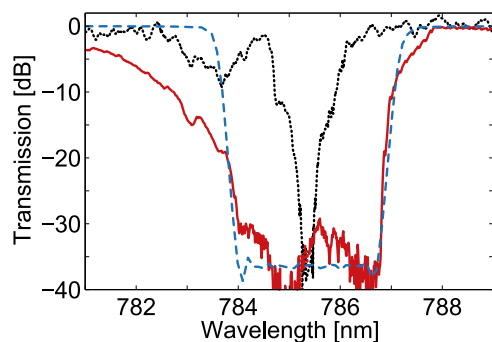
Fig. 9. Measured transmission spectrum of a chirped grating in a 19-core SM-MCF (solid red) in comparison to simulation (dashed blue), and a homogeneous grating (dotted black).

should be mentioned that Eq. (7) indicates that chirped gratings yield but a limited filtering efficiency if one or several individual cores fail to be exposed to light during FBG inscription.

VIII. SUMMARY AND OUTLOOK

A fiber with a hexagonal MCF structure has been demonstrated to serve as an efficient spectral filter in a single-mode MCF which is suitable for the implementation of Bragg gratings. The inscription of FBGs in the presented fiber type is affected mainly by three factors: variation of the core sizes due to manufacturing tolerances as well as focusing effects due to the geometrical structure of the fiber and the core-array. Additionally, UV-absorption causes shadowing effects. It has been shown that, considering the measured distribution of reflection strength and wavelength shift a good agreement between the theory and measurement of the filter characteristic can be achieved. Future applications require more light collecting efficiency. This can be achieved by an increase of the amount of applied waveguides in a single fiber. Grating inscription concepts that increase photosensitivity at decreased absorption would help to homogenize the transversal grating structures which will become even more important for considerably higher core numbers. Novel fiber designs that improve illumination uniformity during grating inscription would also be a significant step forward.

REFERENCES

[1] J. Bland-Hawthorn, S. Ellis, S. G. Leon-Saval, R. Haynes, M. M. Roth, H.-G. Löhmannsröben, A. Horton, J.-G. Cuby, T. Birks, J. Lawrence, P. Gillingham, S. Ryder, and C. Trinh, "A complex multi-notch astronomical filter to suppress the bright infrared sky," *Nat. Commun.*, vol. 2, no. 581, pp. 1–7, 2011.

[2] A. G. Mignani, Ciaccheri, A. A. Mencaglia, R. D. Sanzo, S. Carabetta, and M. Russo, "Dispersive Raman spectroscopy for the nondestructive and rapid assessment of honey quality," *Proc. SPIE*, vol. 9634, pp. 96340U-1–96340U4, 2015.

[3] J. T. Motz, M. Hunter, L. H. Galindo, J. A. Gardecki, J. R. Kramer, R. R. Dasari, and M. S. Feld, "Optical fiber probe for biomedical Raman spectroscopy," *Appl. Opt.*, vol. 43, no. 3, pp. 542–554, 2004.

[4] Y. Komachi, H. Sato, K. Aizawa, and H. Tashiro, "Micro-optical fiber probe for use in an intravascular Raman endoscope," *Appl. Opt.*, vol. 44, no. 22, pp. 4722–4732, 2005.

[5] U. Utzinger and R. R. Richards-Kortum, "Fiber optic probes for biomedical optical spectroscopy," *J. Biomed. Opt.*, vol. 8, no. 1, pp. 121–147, 2003.

[6] F. Knappe, H. Renner, and E. Brinkmeyer, "Efficient design of spatially symmetric Bragg gratings for add/drop multiplexers," *Int. J. Electron. Commun.*, vol. 62, no. 7, pp. 513–520, 2008.

[7] T. A. Birks, B. J. Mangan, A. Diez, J. L. Cruz, and D. F. Murphy, "Photonic lantern—Spectral filters in multi-core fibre," *Opt. Exp.*, vol. 20, no. 13, pp. 13996–14008, 2012.

[8] R. Haynes, T. A. Birks, J. Bland-Hawthorn, J. L. Cruz, A. Diez, S. C. Ellis, D. Haynes, R. G. Krämer, B. J. Mangan, S. Min, D. F. Murphy, S. Nolte, J. C. Olaya, J. U. Thomas, C. Q. Trinh, A. Tünnermann, and C. Voigtländer, "Second generation OH suppression filters using multicore fibres," *Proc. SPIE*, vol. 8450, pp. 845011-1–845011-12, 2012.

[9] S. Min, C. Trinh, S. Leon-Saval, N. Jovanovic, P. Gillingham, J. Bland-Hawthorn, J. Lawrence, T. A. Birks, M. M. Roth, R. Haynes, and L. Fogarty, "Multi-core fiber Bragg grating developments for OH suppression," *Proc. SPIE*, vol. 8450, pp. 84503L-1–84503L-10, 2012.

[10] E. Lindley, S.-S. Min, S. Leon-Saval, N. Cvetojevic, J. Lawrence, S. Ellis, and J. Bland-Hawthorn, "Demonstration of uniform multicore fibre Bragg gratings," *Opt. Exp.*, vol. 22, no. 25, pp. 31575–31581, 2014.

[11] E. Lindley, S.-S. Min, S. Leon-Saval, N. Cvetojevic, N. Jovanovic, J. Bland-Hawthorn, J. Lawrenc, I. Gris-Sanchez, T. Birks, R. Haynes, and D. Haynes, "Core-to-core uniformity improvement in multi-core fiber Bragg gratings," *Proc. SPIE*, vol. 9151, pp. 91515F-1–91515F-9, 2014.

[12] B. E. A. Saleh and M. C. Teich, *Fundamentals of Photonics*, J. W. Goodman, Ed. New York, NY, USA: Wiley, 1991.

[13] T. Mizunami, T. V. Djambova, T. Niiho, and S. Gupta, "Bragg gratings in multimode and few-mode optical fibers," *J. Lightw. Technol.*, vol. 18, no. 2, pp. 230–235, Feb. 2000.

[14] W. Mohammed and X. Gu, "Fiber Bragg grating in large-mode-area fiber for high power fiber laser applications," *Appl. Opt.*, vol. 49, no. 28, pp. 5297–5301, 2010.

[15] J. Thomas, N. Jovanovic, R. G. Becker, G. D. Marshall, M. J. Withford, A. Tünnermann, S. Nolte, and M. J. Steel, "Cladding mode coupling in highly localized fiber Bragg gratings: Modal properties and transmission spectra," *Opt. Exp.*, vol. 19, no. 1, pp. 325–341, 2011.

[16] P. J. Russell, J. L. Archambault, and L. Reekie, "Fiber gratings," *Phys. World*, pp. 41–48, 1993.

[17] Y. Liu, J. Lit, X. Gu, and L. Wei, "Fiber comb filters based on UV-writing Bragg gratings in graded-index multimode fibers," *Opt. Exp.*, vol. 13, pp. 8508–8513, 2005.

[18] S. Dochow, I. Latka, M. Becker, R. Spittel, J. Kobelke, K. Schuster, A. Graf, S. Brückner, S. Unger, M. Rothhardt, B. Dietzek, C. Krafft, and J. Popp, "Multicore fiber with integrated fiber Bragg gratings for background-free raman sensing," *Opt. Exp.*, vol. 20, no. 18, pp. 20156–20169, Aug. 2012.

[19] T. A. Birks, G. J. Pearce, and D. M. Bird, "Approximate band structure calculation for photonic bandgap fibres," *Opt. Exp.*, vol. 14, no. 20, pp. 9483–9490, 2006.

[20] K. Schuster, S. Unger, C. Aichele, F. Lindner, S. Grimm, D. Litzkendorf, J. Kobelke, J. Bierlich, K. Wondraczek, and H. Bartelt, "Material and technology trends in fiber optics," *Adv. Opt. Techn.*, vol. 3, no. 4, pp. 447–468, 2014.

[21] D. L. Franzen, "Determining the effective cutoff wavelength of single-mode fibers: An lnterlaboratory comparison," *J. Lightw. Technol.*, vol. 3, no. 1, pp. 128–134, Feb. 1985.

[22] Y. Murakami, A. Kawana, and H. Tsuchiya, "Cut-off wavelength measurements for single-mode optical fibers," *Appl. Opt.*, vol. 18, no. 7, pp. 1101–1104, 1979.

[23] U. Röpke, H. Bartelt, S. Unger, K. Schuster, and J. Kobelke, "Two-dimensional high-precision fiber waveguide arrays for coherent light propagation," *Opt. Exp.*, vol. 15, no. 11, pp. 6894–6899, 2007.

[24] W. Rasband. (2012). Image - image processing and analysis in java. National Institutes of Health. [Online]. Available: http://rsb.info.nih.gov/ij/

[25] Corning Inc. (2002). *Corning SMF-28 Optical Fiber - Product Information* [Online]. Available: www.corning.com/opticalfiber

[26] U. Röpke, H. Bartelt, S. Unger, K. Schuster, and J. Kobelke, "Fiber waveguide arrays as model system for discrete optics," *Appl. Phys. B*, vol. 104, pp. 481–486, 2011.

[27] A. Ghatak and A. Kumar, *Polarization of Light with Applications in Optical Fibers*. New Delhi, India: Tata McGraw Hill, 2012.

[28] R. M. Atkins, "Measurement of the ultraviolet absorption spectrum of optical fibers," *Appl. Opt.*, vol. 17, no. 7, pp. 469–471, 1992.

[29] R. M. Atkins and V. Mizrahi, "Observation of changes in UV absorption bands of singlemode germanosilicate core optical fibers on writing and thermally erasing refractive index gratings," *Electron. Lett.*, vol. 28, no. 18, pp. 1743–1744, 1992.

[30] I. Ota, T. Tsuda, A. Shinozaki, S. Yodo, T. Ota, T. Shigematsu, and Y. Ibusuki, "Development of optical fiber gratings for WDM systems," *Furukawa Rev.*, vol. 19, pp. 35–40, 2000.

[31] M. Becker, T. Elsmann, I. Latka, M. Rothhardt, and H. Bartelt, "Chirped phase mask interferometer for fiber Bragg grating array inscription," *J. Lightw. Technol.*, vol. 33, no. 10, pp. 2093–2098, May 2015.

[32] P. J. Lemaire, R. M. Atkins, V. Mizrahi, and W. A. Reed, "High pressure H_2 loading as a technique for achieving ultrahigh UV photosensitivity and thermal sensitivity in GeO doped optical fibres," *Electron. Lett.*, vol. 19, no. 13, pp. 1191–1193, 1993.

[33] C. M. Rollinson, S. A. Wade, B. P. Kouskousis, D. J. Kitcher, G. W. Baxter, and S. F. Collins, "Variations of the growth of harmonic reflections in fiber Bragg gratings fabricated using phase masks," *J. Opt. Soc. Amer. A*, vol. 29, no. 7, pp. 1259–1268, 2012.

[34] C. W. Smelser, D. Grobnic, and S. J. Mihailov, "Generation of pure two-beam interference grating structures in an optical fiber with a femtosecond infrared source and a phase mask," *Opt. Lett.*, vol. 29, no. 15, pp. 1730–1732, 2004.

[35] H. Sorensen, J. Canning, J. Laegsgaard, K. Hansen, and P. Varming, "Liquid filling of photonic crystal fibres for grating writing," *Opt. Commun.*, vol. 270, pp. 207–210, 2007.

[36] V. B. Martins, "Caracterisação de redes de Bragg em fibras óticas microestructuradas multicore," Bachelor's Thesis, Universidade Federal de São Carlos, São Carlos, Brazil, 2014.

[37] R. Mahakud, O. Prakash, J. Kumar, S. V. Nakhe, and S. K. Dixit, "Analysis on the effect of UV beam intensity profile on the refractive index modulation in phase mask based fiber Bragg grating writing," *Opt. Commun.*, vol. 285, pp. 5351–5358, 2012.

[38] J. L. Cruz, L. Dong, S. Barcelos, and L. Reekie, "Fiber Bragg gratings with various chirp profiles made in etched tapers," *Appl. Opt.*, vol. 35, no. 34, pp. 6781–6787, 1996.

Authors' biographies not available at the time of publication.